KEK Preprint 2000-143
February 2001
H

Active Target with Plastic Scintillating Fibers for Hyperon-Proton Scattering Experiments

J.K. AHN, H. AKIKAWA, J. ARVIEUX, B. BASSALLECK, M.S. CHUNG, H. EN'YO, T. FUKUDA, H. FUNAHASHI, S.V. GOLOVKIN, A.M. GORIN, Y. GOTO, M. HANABATA, T. HAYAKAWA, A. ICHIKAWA, M. IEIRI, K. IMAI, M. ISHINO, H. KANDA, Y.D. KIM, Y. KONDO, E.N. KOZARENKO, I.E. KRESLO, J.M. LEE, A. MASAIKE, S. MIHARA, K. NAKAI, K. NAKAZAWA, K. OZAWA, A. SATO, H.D. SATO, K.S. KIM, T. TABARU, F. TAKEUTCHI, P. TLUSTY, H. TORII, K. YAMAMOTO, S. YOKKAICHI and M. YOSHIDA

Submitted to IEEE Trans. Nucl. Sci.

High Energy Accelerator Research Organization (KEK)

KEK Reports are available from:

Information Resources Division
High Energy Accelerator Research Organization (KEK)
1-1 Oho, Tsukuba-shi
Ibaraki-ken, 305-0801
JAPAN

Phone: +81-298-64-5137
Fax: +81-298-64-4604
E-mail: irdpub@mail.kek.jp
Internet: http://www.kek.jp

Active Target with Plastic Scintillating Fibers for Hyperon-Proton Scattering Experiments

J. K. Ahn, H. Akikawa, J. Arvieux, B. Bassalleck, M. S. Chung, H. En'yo, T. Fukuda, H. Funahashi, S. V. Golovkin, A. M. Gorin, Y. Goto, M. Hanabata, T. Hayakawa, A. Ichikawa, M. Ieiri, K. Imai, M. Ishino, H. Kanda, Y. D. Kim, Y. Kondo, E. N. Kozarenko, I. E. Kreslo, J. M. Lee, A. Masaike, S. Mihara, K. Nakai, K. Nakazawa, K. Ozawa, A. Sato, H. D. Sato, K. S. Sim, T. Tabaru, F. Takeutchi, P. Tlusty, H. Torii, K. Yamamoto, S. Yokkaichi, M. Yoshida

Abstract-- **An active target with plastic scintillating fibers has been constructed. This active target serves as a production target of hyperons as well as a scattering target, and works as a 4π-detector for charged particles. This system is designed for measurements of hyperon-proton scattering for hyperon momenta of several hundred MeV/c. A spectrometer system for the incident beam and outgoing particles of the hyperon production reaction is linked with this target-detector in order to provide triggers for the imaging device of this detector system. As a control of this detector, the decay constant of Σ^- hyperon has been evaluated.**

I. Introduction

Recent progress in scintillating fiber technology has made it possible to design new types of visual detector assemblies[1]. We have developed an active target with block of scintillating fibers (SCIFI) in order to measure hyperon-proton (Yp) scattering [2],[3], which is viewed by two chains of image intensifiers (IIs) to reconstruct three-dimension reaction kinematics of the event inside the SCIFI block. The existing data of Yp scattering are from bubble-chamber experiments performed in the 1960's [4]. In recent nuclear physics experiments concerning strangeness, a precise tracking of hyperons decays plays an essential role in order to obtain information about the event, itself, or about the reaction sequence [5].

The SCIFI block target and the imaging device are explained in sect. 2 and 3, respectively. The process of treating image data is described in sect. 4. In sect. 5, the analysis of Σ^- production events is mentioned, and the decay

The corresponding author, M. Ieiri, is with IPNS, KEK, High Energy Accelerator Research Organization, Oho 1-1, Tsukuba 305-0801, Japan (telephone +81-298-64-5638, e-mail: masaharu.ieiri@kek.jp).

J. K. Ahn was with the Department of Physics, Kyoto University, Kyoto 606-8502, Japan. He is now with Research Center for Nuclear Physics, Osaka University, Ibakaki, Osaka 567-0047, Japan.

H. Akikawa, H. En'yo, H. Funahashi, A. Ichikawa, K. Imai, H. D. Sato, T. Tabaru, H. Torii and S. Yokkaichi are with the Department of Physics, Kyoto University, Kyoto 606-8502, Japan.

J. Arviuex was with the Laboratoire National Saturne, F-91191, Gif-sur-Yvette, CEDEX, France. He is now with Institut de Physique Nucleaire, Universite Paris-Sud, F-91406 ORSAY-Cedex, France.

B. Bassalleck is with Department of Physics, University of New Mexico, Albuquerque, N.M. 87131, U.S.A.

M. S. Chung was with Department of Physics, Kyoto University, Kyoto 606-8502, Japan. He is now with P-25, MS H846, Los Alamos National Laboratory, Los Alamos, NM 87545, U.S.A.

T. Fukuda is with IPNS, KEK, High Energy Accelerator Research Organization, Oho 1-1, Tsukuba 305-0801, Japan.

S. V. Golovkin and A. M. Gorin are with Institute for High Energy Physics, RU-142284, Protvino, Russia.

Y. Goto and M. Yoshida were with the Department of Physics, Kyoto University, Kyoto 606-8502, Japan. They are now with RIKEN, Institute of Physical and Chemical Research, Wako, Saitama 351-0198, Japan.

M. Hanabata and K. Nakazawa are with Physics Department, Gifu University, Gifu 501-1193, Japan.

T. Hayakawa was with Department of Physics, Science University of Tokyo, Chiba 278-8510, Japan. He is now with Central Japan Railway Company, Meieki 1-1-4, Nakamura, Nagoya, Aichi, 450-6101, Japan.

M. Ishino and S. Mihara were with Department of Physics, Kyoto University, Kyoto 606-8502, Japan. They are now with International Center for Elementary Particle Physics, University of Tokyo, Tokyo 113-0033, Japan.

H. Kanda was with Department of Physics, Kyoto University, Kyoto 606-8502, Japan. He is now with Physics Department, Graduate School of Science, Tohoku University, Sendai 980-8578, Japan.

Y. D. Kim was with Physics Department, Seoul National University, Seoul 151-742, Korea. He is now with Physics Department, Sejong University, Seoul, 143-747, Korea.

Y. Kondo was with Department of Physics, Kyoto University, Kyoto 606-8502, Japan. He is now with Accelerator Laboratory, KEK, High Energy Accelerator Research Organization, Oho 1-1, Tsukuba 305-0801, Japan.

E. N. Kozarenko and I. E. Kreslo are with Joint Institute for Nuclear Research, RU-141980, Dubna, Russia.

J. M. Lee was with Department of Physics, Yonsei Univ., Seoul 120-749, Korea. He is now with Korea Research Institute of Standards and Science, 1 Toryong-dong, Yusong-gu, Taejoen 305-600, Korea.

A. Masaike was with Department of Physics, Kyoto University, Kyoto 606-8502, Japan. He is now with Fukui University of Technology, Fukui 910-8505, Japan.

K. Nakai and S. Sato are with Department of Physics, Science University of Tokyo, Chiba 278-8510, Japan.

K. Ozawa was with Department of Physics, Kyoto University, Kyoto 606-8502, Japan. He is now with Center for Nuclear Study, University of Tokyo, Tokyo 113-0033, Japan.

K. S. Sim is now with Department of Physics, Korea University, Seoul 136-701, Korea.

F. Takeutchi is with Department of Physics, Kyoto Sangyo University, Kyoto 603-8555, Japan.

P. Tlusty is with Nuclear Physics Institute, 250 68 Rez, Czech Republic.

K. Yamamoto was with Department of Physics, Kyoto University, Kyoto 606-8502, Japan. He is now with Department of Physics, Osaka City University, Osaka 558-8585, Japan.

constant of Σ^- is deduced as a control of the detector system. A summary is presented in sect. 6.

II. Scintillating Fiber Block Target

The SCIFI block consists of plastic scintillating fibers, KURARAY SCSF-78 [6]. Each fiber is 30 cm long and has a 300 μm × 300 μm square cross section. The core of the fiber is 288 μm × 288 μm square, which is coated with a 6 μm thick cladding.

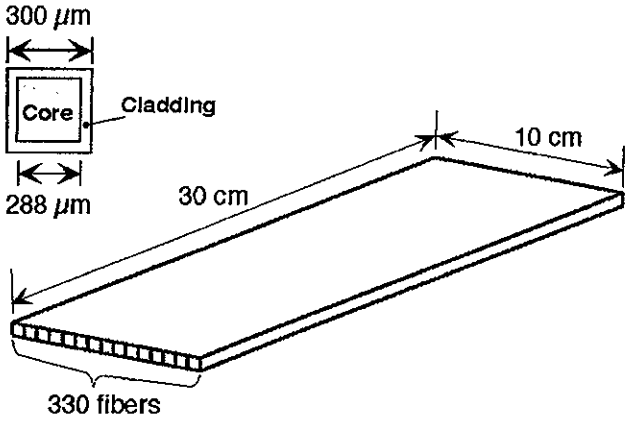

Fig. 1. Schematic drawing of (a) the cross section of a fiber and a fiber sheet, (b) the structure of the SCIFI block. The SCIFI block is assembled by stacking alternate fiber sheets.

The SCIFI block is assembled by stacking alternate fiber-sheets, as shown in Figs. 1-(a) and (b). Each fiber sheet consists of about 330 fibers, corresponding to 100 mm in width. The fiber sheets are bonded with white water paint, which eliminates any cross talk across the fiber-sheets by diffused reflection of the untrapped photons. The overlapping area between alternate fiber sheets is 100×100 mm^2. About 600 sheets are stacked to form an effective target thickness of 200 mm along the beam direction. The fiber sheets in each direction are bundled and polished at the readout arms to make readout surfaces of 100×100 mm^2. The effective volume serving as an active target is the overlapping area of 100×100 mm^2 with 200 mm thickness in the beam direction.

Photons created by the interaction of a charged particle in a fiber reach the end of each fiber, and those end-surfaces make a line of bright points as the projected track of a charged particle. By using two sets of these projected tracks in the U-Z and V-Z plane of the SCIFI block, we reconstruct three-dimensional track(s) of charged particle(s) in the target volume, and the kinematics of the reaction inside the SCIFI target is calculated by these reconstructed tracks together with the track and momentum information of the incident pion and outgoing kaon of the hyperon production reaction obtained by the spectrometer system.

III. Image Intensifier Tubes

Photons from the projected track of charged particles in the SCIFI block are amplified by IIs. Two sets of the II chain are attached at the readout arms for the U-Z and V-Z planes of the SCIFI block. A chain of IIs is shown in Fig. 2.

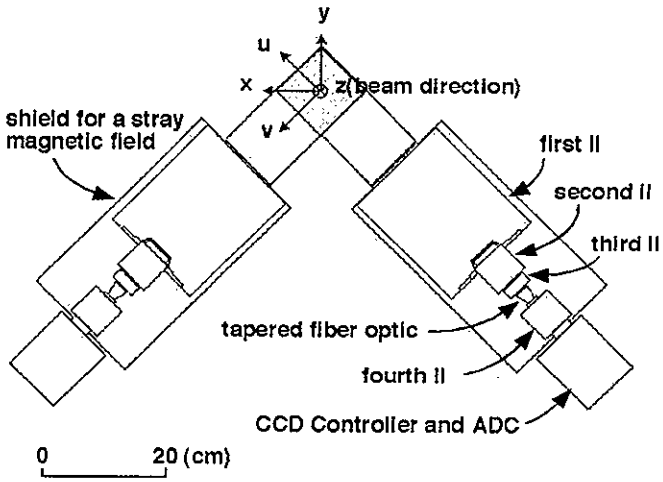

Fig. 2. SCIFI target viewed by two chains of IIs. The first (V4440PX : HAMAMATSU [7]) and the second (PP0030X : DEP [8]) stages are of the electrostatic type. The third stage (BV2563McG : PROXITRONIC [8]) is of the micro channel plate (MCP) type. At the fourth stage, an electron bombarded CCD (EBCCD : GEOSPHAERA [9]) is employed. A tapered fiber optic (HOYA-SCHOTT [10]) is used between the third stage and the fourth stage to match the image size to the sensitive area of the CCD.

The third II and the electron bombarded CCD (EBCCD) are operated in the gate mode by independent external triggers, which are created by fast detectors of the spectrometer syetem (SP) consisting of a dipole magnet, several wire chambers, an aerogel Cherenkov counter, a hodoscope, and a TOF array. The external triggers consist of two different levels. The 1st level trigger, made by fast signals from photomultipliers of SP, opens the third MCP gate. The 2nd level trigger, called

"mass trigger", is determined by momentum and time-of-flight information by the hodoscope and the TOF array, to open the EBCCD gate. The image data from the CCD are digitized in real time with a 6-bit flash-ADC. The digitized data are compressed with a compactor module in a CAMAC crate. A typical example of the image for Σ^-p scattering is shown in Fig. 3. The average data size is about 7 kbyte/image. Details concerning the IIs chain and triggers made by detectors of the SP are described in ref. [2],[11].

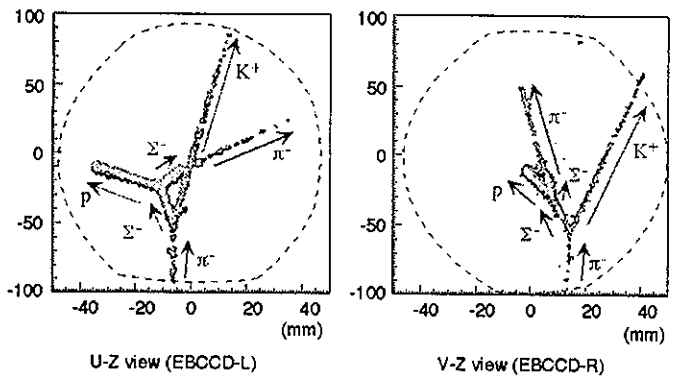

Fig. 3. U-Z and V-Z view of a Σ-p scattering event.

IV. Image Data Analysis

A. Analysis procedure

Raw image data are distorted by the pin-hole distortion of the electrical lens system and a stray field from SP. First among all processes, this distortion should be corrected.

To derive the observed values and their errors, the efficiencies and accurateness of the analysis should be estimated. For this purpose, Monte-Carlo simulations were performed. Simulated image data were generated and analyzed through the same process as the real data.

Then, pictures are eye-scanned and categorized according to the event patterns. The events including visible Σ^-'s are selected and used for further analysis. After categorization is completed, the reaction points are marked on a graphic display with a pointing device.

B. Position calibration

Raw images on the CCD suffer a pin-hole distortion caused by the electrical lens system of the IIs. A Stray field from SP also distorts the images. The actual position of each pixel in the SCIFI target is compensated by placing a black lucite-plate with holes on the opposite side end of the SCIFI block, and uniformly illuminating them with an electro-luminescence panel from outside. Fig. 4 shows pictures of calibration patterns before and after a correction.

The diameter of the hole is 300μmϕ, and the pitches are 10mm and 5mm longitudinal and transverse to the beam direction, respectively. The pixel position is transformed to the real position with a formula obtained by using a two-dimensional spline fitting. The centers of the holes are aligned with an accuracy of 50 μm after compensation.

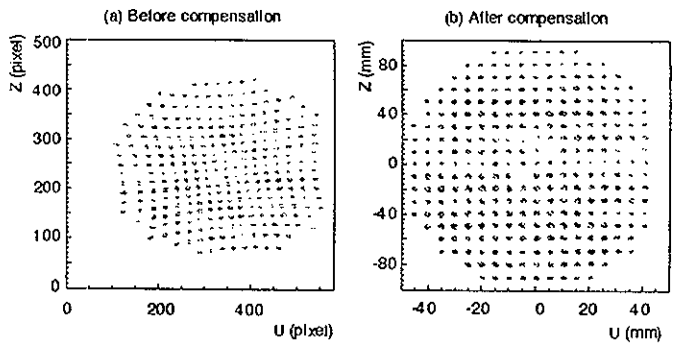

Fig.4. Position compensation by using a calibration pattern illuminated with an electro-luminescence panel. (a) A picture of the raw pattern. (b) After compensation, the scales are converted to the real dimension in the SCIFI block.

C. Image Data Simulation

In order to estimate the analyzing efficiencies and accurateness of pointing and to evaluate systematic errors, a Monte-Carlo simulation was performed by using GEANT 3 [12]. To evaluate the scanning efficiency, the simulated image data were mixed into the real data. The Σ^-'s were generated by the $\pi^- + (p) \rightarrow K^+ + \Sigma^-$ reaction, and scatter or react with protons in the simulation. The Fermi motion in carbon nuclei was reproduced with the distribution as

$$N(p) = \frac{N_0}{1 + \exp\left(\frac{p(GeV/c) - 0.1}{0.05}\right)} . \qquad (1)$$

The energy loss of the charged particles, an effect of multiple Coulomb scattering, was calculated by GEANT. The response of the SCIFI detector system was simulated to reproduce the characteristics of the real tracks, and simulated image data were created. Finally, the brightness distributions of π^- and Σ^- tracks and their track width were well reproduced.

The generated image data were analyzed through the same process as the real data, and the efficiencies were evaluated from the surviving rate of the simulation events. The angular resolution and the accuracy of the track-length measurements were also estimated using the simulation data by comparing the generated positions to the positions obtained by the pointing process.

V. Analysis of Σ^- Production and its Decay Constant

A. Σ^-p elastic scattering experiment

We have performed Σ^-p elastic scattering. Σ^-'s of 400 to 700 MeV/c were produced through the in-flight p(π^-, K^+) Σ^- reaction in the SCIFI with a 1.32 GeV/c π^- beam. Subsequent elastic scattering of Σ^- hyperons was observed in the SCIFI active target. Details of the analysis of Σ^-p elastic scattering

are described in ref. [2]. Here, we explain an analysis of the Σ^- hyperon production reaction, which is important for obtaining the absolute value of the cross sections of Σ^-p elastic scattering, since the produced Σ^-'s act as a "beam" for Σ^-p scattering.

B. Requirement for Σ Production

For 2947 event samples of the Σ^- beam candidates, the reaction points were marked on a graphic display with a pointing device (the pointing process) to evaluate the amount of "Σ^- beam". This corresponds to 1.6% of all the data in the Σ^-p scattering experiment. A typical Σ^- production event is shown in Fig. 5.

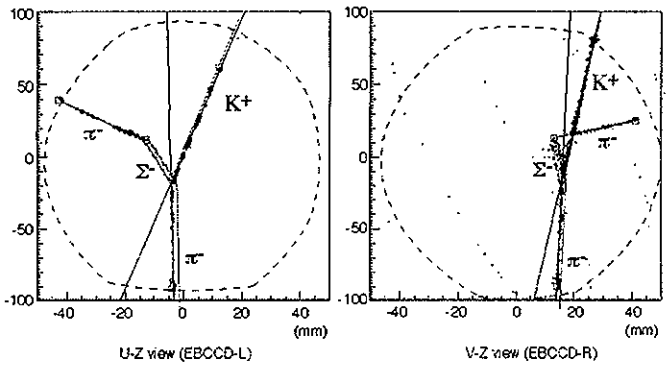

Fig. 5. Example of a Σ^- production event observed with the SCIFI detector. The open squares represent the input positions given in the pointing process. The solid lines just on the π^- and K^+ tracks are the fitted lines, and the dotted lines slightly deviating from the tracks represent the predicted tracks with the external wire chambers.

The weak decay of $\Sigma^- \rightarrow \pi^- n$ was easily recognized in the pointing process, because the brightness of the Σ^- and π^- tracks was quite different. The starting point of the Σ^- track was the vertex point of the (π^-, K^+) reaction and the end point was the kinked point or the point where the brightness of the track suddenly changed.

The production vertex of the (π^-, K^+) reaction was reconstructed by using the image data. The vertex position was defined as the closest point of the Σ^- and K^+ tracks. The vertex resolution along the z-axis was estimated to be 0.6 mm from the simulation data.

The measurement error of the track length of the Σ^- causes systematic errors in the cross section. Additionally, if the length of the Σ^- is too short, the event selection becomes ambiguous. Fig. 6-(a) shows the difference of the flight length between the generated one by the simulation and the measured one by the pointing process. Fig. 6-(b) shows the efficiencies for the event categorization, pointing and kinematical cut to select the H-target Σ^- beam as a function of the flight length of the Σ^-. The definition of the H-target Σ^- beam and the details of the kinematical cut are described below. The Σ^- whose flight length was longer than 5mm was used for the Σ^- beam. To avoid ambiguities in the categorization for events which occurred at the upstream and downstream ends of the SCIFI, the z-position of the vertex was required to be within -90 mm ~ 60 mm, where the origin of the coordinate was the center of the SCIFI block.

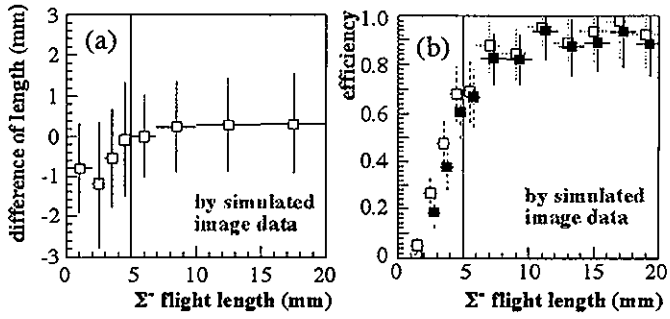

Fig. 6. Σ^- flight length dependence of (a) the error of length obtained by the pointing process, and (b) the analyzing efficiency. In figure (b), open squares represent the efficiency of the event categorization and pointing, and closed squares represent the total efficiency including the kinematical cut efficiency to select the H-target Σ^- beam (The definition of H-target is described in the next subsection.) They were obtained with the analysis of the simulated image data. The threshold value for the Σ^- track length was set to 5mm, as indicated by the lines in the figure.

C. Σ Produced on Free Protons and Carbon Nuclei

Since the SCIFI target consisted of (CH)n, Σ^-'s were produced both on free protons (hydrogen target) and carbon nuclei (carbon target). We call them the H-target and C-target Σ^- beams, respectively. For the C-target beam, the momentum of the Σ^- beam is not well determined by the (π^-, K^+) kinematics due to the Fermi motion.

In order to separate the H-target Σ^- beam, we adopted the H-target cut, which includes the angle-difference and missing-mass cuts. The angle-difference for the Σ^- production kinematics ($\Delta\theta_{prod}$) was defined as

$$\Delta\theta_{prod} = \cos^{-1}\left(\frac{p_{\Sigma^- prod} \cdot d_{\Sigma^- prod}}{\left|p_{\Sigma^- prod}\right|\left|d_{\Sigma^- prod}\right|}\right) \qquad (2)$$

where, $d_{\Sigma^- prod}$ is the measured direction of the Σ^- obtained from the pointing process, and $p_{\Sigma^- prod}$ denotes the predicted momentum vector of the Σ^- calculated from the momentum vectors of the π^- and the K^+. The momenta of the π^- and K^+ were obtained from an analysis of the spectrometer data, and the directions were measured with the SCIFI detector and the external wire chambers. The energy loss in the SCIFI target was taken into account to calculate the production kinematics.

Fig. 7-(a) shows the distribution of $\Delta\theta_{prod}$ versus the flight length of the Σ^- (fl_{Σ^-}). The $\Delta\theta_{prod}$ distribute around zero within the resolution of the SCIFI system for the H-target Σ^- beam. These events make a narrow peak, and which can be distinguished from the broader distribution of the C-target Σ^- beam. The region inside the lines in Fig. 7-(a) was the

accepted region for the Σ^-'s produced on free protons. The threshold was set to be

$$\Delta\theta_{prod} < \frac{1.35}{fl_{\Sigma^-}} + 0.03, \quad fl_{\Sigma^-} > 5mm \qquad (3)$$

by taking projections of Fig. 7-(a) onto $\Delta\theta_{prod}$ in some slices of (fl_{Σ^-}).

Fig. 7-(b) shows the missing-mass spectrum of the p(π^-, K^+)X reaction (MM_{prod}) after the angle-difference cut was applied. The missing-mass resolution was 7.4 MeV/c^2 (r.m.s.). The criterion for the missing-mass cut was

$1.174 < MM_{pro} < 1.218$ (GeV/c^2). (4)

The events which satisfy (3) and (4) were regarded as the H-target Σ^- beam, and the other events were recognized as the C-target Σ^- beam. The contamination from the C-target in the H-target Σ^- beam was estimated to be 10% from Fig. 7-(b).

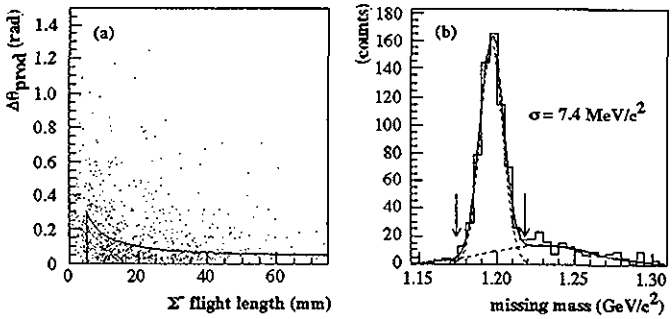

Fig. 7. (a) Scatter plot of $\Delta\theta_{prod}$ versus the flight length of the Σ^- (fl_{Σ^-}). (b) Missing-mass spectrum of the p(π^-, K^+)X reaction after the angle-difference cut was applied. The lines on the spectrum are obtained with a two-Gaussian fitting. The events inside the region indicated by the arrows were regarded as the Σ^-'s produced on free protons (H-target Σ^- beam).

D. Lifetime of Σ

To confirm the Σ^- event selection and test the detector system, the lifetime of the Σ^- was derived as follows.

The mean flight length, x, of the particle with the lifetime τ is given by

$$x = c\tau \cdot \beta\gamma = c\tau \cdot \frac{p}{m}, \qquad (5)$$

where m and p are the mass and momentum of the particle, respectively. For charged particles in material, the energy loss of the particle along its path should be taken into account, then, $x \cdot m/p$ is replaced by L, which is defined as

$$L = \int_0^x \frac{m}{p(\xi)} \cdot d\xi \,. \qquad (6)$$

The decay rates as a function of L before and after the efficiency correction were evaluated in the region of L between 10 mm and 100 mm, as shown in Fig. 8. The efficiency for each bin of L was obtained by using the simulation data. The decay constant was calculated with the logarithmic likelihood method.

The result is

$c\tau$ = 43.3 ± 3.2 mm, (7)

which is consistent with the known value [13]: $c\tau$ = 44.34 ± 0.33 mm.

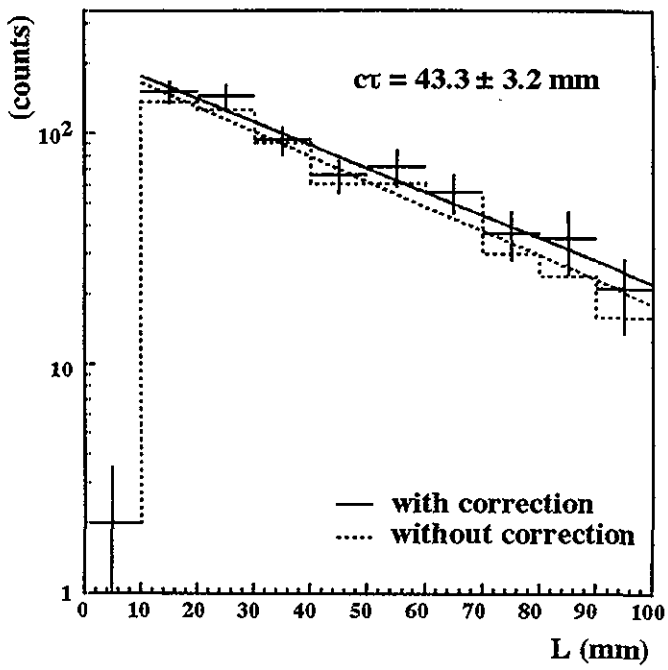

Fig. 8. Distribution of the Σ^- flight length for the H-target Σ^- beam

VI. SUMMARY

A new active target with plastic scintillating fibers has been constructed for hyperon-proton scattering. The SCIFI block consists of 2×10^5 plastic scintillating fibers, KURARAY SCSF78, where each fiber is 30 cm long and has a 300 μm × 300 μm square cross section. 600 sheets, 10 cm wide and 30 cm long with 330 fibers each, are stacked alternately so as to form an effective target volume of 10 × 10 × 20 cm^3. This fiber block is viewed from two orthogonal directions by two sets of II chains. The data are stored as two CCD images, in order to reconstruct the particle trajectories inside the target three-dimensionally.

To evaluate the scanning efficiency of image data, the simulated image data are mixed into the real data. The decay time of Σ^- hyperon is well obtained as a control of this detector system.

VII. ACKNOWLEDGMENT

The dedication and support of many of the KEK staff during this development are very much appreciated. We would like to thank Professors H. Sugawara, S. Yamada, K. Nakamura, and Y. Yoshimura for their continuous encouragement throughout this work. We also thank the KEK accelerator crew and the beam channel group members for their continuous tuning and the stable operation of the machines. This work was supported partially by Grants-in

Aid for Scientific Research no. 06640425 of Japan Ministry of the Education, Science and Culture.

VIII. REFERENCES

[1] SCIFI97; edited by A. D. Bross, R. C. Ruchti, M. R. Wayne, AIP Conference Proceedings 450, 1998.
[2] Y. Kondo, J. K. Ahn, H. Akikawa, J. Arviuex, B. Bassalleck, M. S. Chhung et al., Nucl. Phys. A676, 2000, pp.371-387.
[3] J. K. Ahn, B. Bassalleck, M. S. Chung, W. M. Chung, H. En'yo, T. Fukuda et al., Nucl. Phys. A648, 1999, pp. 263–279.
[4] R. Engelmann, H. Filthuth, V. Hepp, and E. Kluge , Phys. Lett. 21, 1966, pp.587-589; G. Alexander, U. Karshon, A. Shapira and G. Yekutieli, Phys. Rev. 173, 1968, pp.1452-1460; B. Sechi-Zorn, B. Kehoe and J. Twitty, Phys. Rev. 175, 1968, pp.1735-1740; G. R. Charlton, J. Badier, E. Barrelet, I. Makarovisch, J. Pernegr, J. R. Hubbard et al., Phys. Lett. 32B, 1970, pp.720-722; J. A. Kadyk, G. Alexander, J. H. Chan, P. Gaposchkin, G. H. Trilling, Nucl. Phys. B27, 1971, pp.13-22; F. Eisele, H. Filthuth, W. Fohlisch, V. Hepp, G. Zech, Phys. Lett. 37B, 1971, pp.204-206; J. M. Hauptman J. A. Kadyk and G. H. Trilling, Nucl. Phys. B125, 1977, pp.29-51.
[5] J. K. Ahn, S. Aoki, K. S. Chung, M. S. Chung, H. En'yo, T. Fukuda et al., Phys. Lett. B378, 1996, pp.53-58
[6] KURARAY Co. Ltd., Kurashiki 2-28, Nakajo, Kitakanbara, Niigata 959-2653, Japan.
[7] Hamamatsu Co. Ltd., Toyooka Factory, Shimokanzo 314-5, Toyooka, Iwata, Shizuoka 438-0193, Japan.
[8] DHT Co. Ltd., 1-636 Maruko-doori, Nakahara, Kawasaki, Kanagawa 211-0006, Japan.
[9] GEOSPHAERA Inc., Vinitskaya 3/136, Moscow 117192, Russia.
[10] HOYA-SCHOTT Co. Ltd., Shinjuku 3-23-7 , Tokyo 160-0022, Japan.
[11] J. K. Ahn, H. Akikawa, J. Arviuex, B. Bassalleck, M. S. Chung, H. En'yo et al., Nucl. Instr. Meth. 457, 2001, pp.137-150.
[12] GEANT – Detector Description and Simulation Tool, CERN Program Libraly Long Writeup W5013.
[13] Particle data group, Eur. Phys. J. C15, 2000, pp. 1-878.